lubricants

MDPI

Article

Synthesis and Tribological Properties of Multifunctional Nitrogen-Containing Heterocyclic Dialkyl Dithiocarbamate Derivatives

Mengxuan Wang [1,2,3], Ting Li [2], Zhongxian Li [1], Wenjing Hu [1,2,*], Junwei Wang [1,*] and Jiusheng Li [2]

[1] High & New Technology Research Center of Henan Academy of Sciences, Zhengzhou 450008, China
[2] Laboratory for Advanced Lubricating Materials, Shanghai Advanced Research Institute, Chinese Academy of Sciences, Shanghai 201210, China
[3] School of Chemistry and Chemical Engineering, Shihezi University, Shihezi 832003, China
* Correspondence: huwj@sari.ac.cn (W.H.); wjwqabc@163.com (J.W.)

Abstract

Energy conservation and efficiency enhancement necessitate continuous advancement in the development and preparation of multifunctional, high-performance lubricant additives. This paper reports three novel ashless, phosphorus-free, multifunctional nitrogen-containing heterocyclic dialkyl dithiocarbamate derivative additives (Py-2-DBDTC, PDM-DBDTC, and BZT-DBDTC). Thermal stability, oxidation resistance, and tribological properties were investigated for the synthesized additives. All three additives demonstrated excellent thermal stability and oxidation resistance. Furthermore, their extreme-pressure properties improved by 116.33% or more compared to the base oil, while wear reduction rates also exceeded 58.32%. Under both point-to-point and point-on-flat friction conditions, the friction-reducing performance of all three additives was equally outstanding. Across a broad temperature range (25 °C–150 °C), all additives maintained their friction-reducing properties. Analysis of the worn surface morphology reveals that all three additives undergo tribochemical reactions during the friction process, forming tribofilms containing sulfur elements. Research indicates that introducing different nitrogen-containing heterocyclic structures into dialkyl dithiocarbamates can effectively enhance the adsorption capacity of the additives on metal surfaces and promote the formation of tribofilms at the friction interface, thereby significantly improving tribological performance. These systematic investigations not only provide important guidance for the molecular design and industrial application of multifunctional lubricant additives but also further advance the development of sustainable lubrication technologies.

Keywords: nitrogen-containing heterocycles; dialkyl dithiocarbamate; oxidation resistance; tribological property; high-temperature performance

Check for updates

Received: 24 November 2025
Revised: 8 January 2026
Accepted: 10 January 2026
Published: 14 January 2026

Copyright: © 2026 by the authors. Licensee MDPI, Basel, Switzerland. This article is an open access article distributed under the terms and conditions of the Creative Commons Attribution (CC BY) license.

1. Introduction

The development of modern industry depends on the efficient operation of mechanical systems, in which friction and wear between components result in significant energy losses and increase the likelihood of mechanical failure [1–5]. To address these issues, the application of lubricating oil to friction- and wear-prone parts provides a straightforward and efficient solution [6–8]. Lubricants typically comprise a base oil and additives, with the latter playing a central role. These additives are diverse, including extreme-pressure agents, anti-wear agents, friction modifiers, and antioxidants [9,10]. They enhance the overall lubrication performance through synergistic effects [11]. However, the

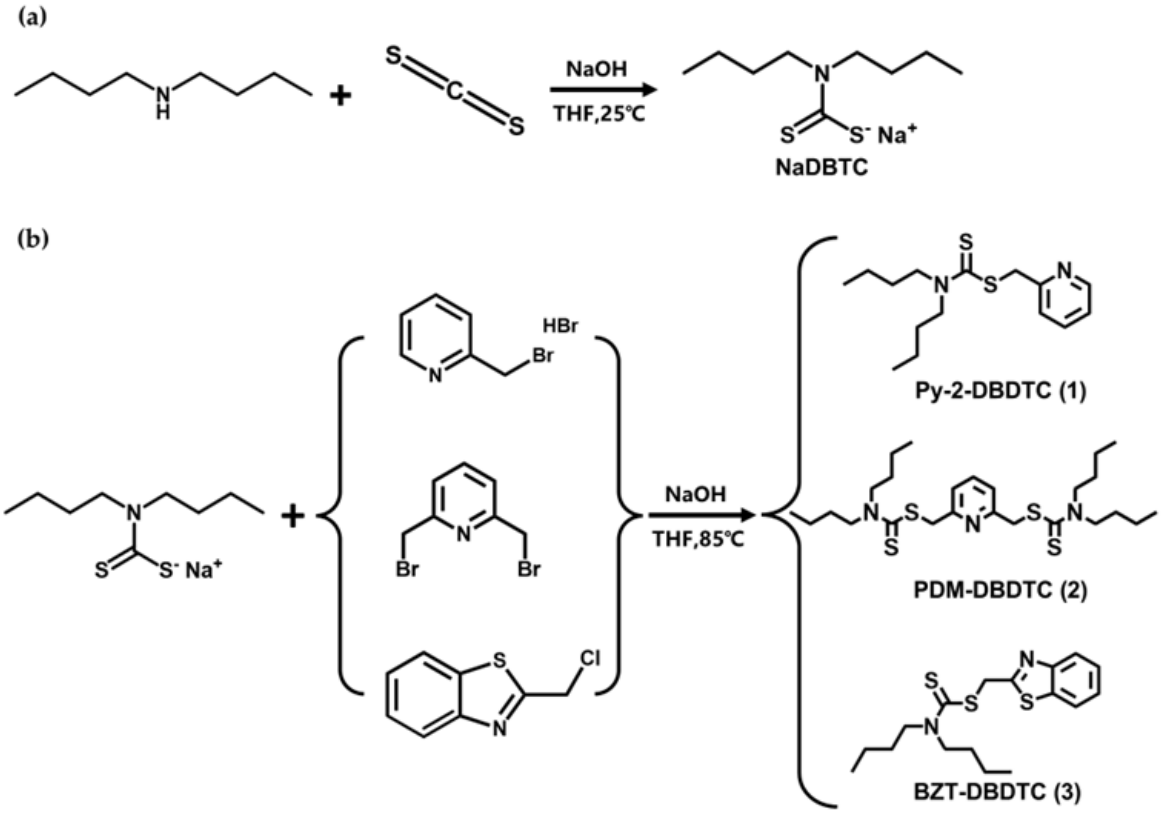
mechanisms of different additives vary and are often complex and difficult to elucidate in depth [12,13]. Therefore, while exerting positive effects, different additives may also introduce unpredictable antagonistic interactions. In this context, multifunctional lubricant additives integrate multiple tribological properties into a single component. This strategy not only effectively avoids potential antagonistic effects between individual additives but also simplifies the complex formulation process, thereby improving application efficiency [14–16].

As a typical multifunctional lubricant additive, zinc dialkyl dithiophosphate (ZDDP) has been widely used in various friction conditions [17,18], yet the P in its structure generates ash that can clog oil pipelines, while the Zn may cause adverse effects such as electrochemical corrosion on metal components, thereby increasingly highlighting its limitations [19,20]. In contrast, dialkyl dithiocarbamate derivatives feature an ash-free and phosphorus-free composition. Containing both N and S in their structure, they promote the adsorption of additive molecules onto metal surfaces during the friction process and undergo tribochemical reactions with the metal substrate to form a chemical reaction film, thereby exhibiting multiple tribological properties. For instance, Y.-W. Kim et al. [21] synthesized a series of dibutyl dithiocarbamate derivatives with varying alkyl chain lengths and evaluated their tribological performance, confirming their excellent thermal stability. Surface analysis indicated that sulfur atoms reacted with iron oxides on the metal surface during friction to form a tribofilm, resulting in outstanding anti-wear and friction-reducing properties. Similarly, Huang et al. [22] prepared three thiazole-based dialkyl dithiocarbamate derivatives, which were shown to improve extreme-pressure resistance, anti-wear performance, and friction reduction. Wear surface analysis revealed that nitrogen adsorbed onto the lubricated surface, while sulfur chemically reacted with the metal to form a reaction film containing sulfates, organic sulfur compounds, and FeS_2, collectively contributing to their tribological effectiveness through both physical adsorption and chemical film formation.

Building on the structural features of the dialkyl dithiocarbamate group, structural modification through the introduction of different polar functional groups to further enhance the tribological properties of dialkyl dithiocarbamate derivatives has become a current research focus. Nitrogen-containing heterocyclic compounds, in particular, have attracted attention due to their stable cyclic structures, which not only confer excellent load-bearing capacity and tribological performance but also provide good high-temperature stability [23,24]. For example, Zhang et al. [25] designed and synthesized two triazine-based derivatives as organic friction modifiers and investigated their tribological performance under high-temperature conditions. The results indicated that these derivatives can effectively adsorb onto the substrate surface, reducing friction and wear, while maintaining outstanding anti-friction properties even at elevated temperatures. Similarly, Zeng et al. [26] synthesized two ash-free and phosphorus-free hydroxyl-containing dithiocarbamate-triazine compounds. Experimental results demonstrated that both additives exhibit high thermal stability in rapeseed oil. Mechanistic analysis revealed that during boundary sliding, the additives form a protective film on the metal surface composed of inorganic sulfides, sulfates, oxidized compounds, and organic nitrogen-containing compounds, thereby endowing the lubricant with excellent extreme-pressure, anti-wear, and friction-reducing properties. Furthermore, Xiong et al. [27] synthesized two nitrogen-containing heterocyclic imidazoline compounds and studied their tribological, antirust, and anti-corrosion properties as additives in water–glycol fluid. The findings showed that these additives possess favorable corrosion resistance, extreme-pressure performance, and anti-wear capabilities. Analysis suggested a synergistic tribological effect between the nitrogen-containing heterocyclic group and the imidazoline group, with the presence of organic nitrogen compounds, iron

oxides, and sulfides in the friction film identified as key factors contributing to the improved tribological performance.

By integrating the performance advantages of thiocarbamates and nitrogen-containing heterocyclic compounds, this study designed and synthesized a series of novel ashless, phosphorus-free multifunctional nitrogen-containing heterocyclic dialkyl dithiocarbamate lubricant additives, whose molecular structures are depicted in Scheme 1. Through the strategic reaction of dialkyl dithiocarbamates with halides of compounds containing heterocycles, such as pyridine and benzothiazole, derivatives with different nitrogen heterocycles or varying numbers of dialkyl dithiocarbamate groups were designed and obtained. Their structure–activity relationships were investigated, and the lubrication mechanism was studied through wear surface analysis.



Scheme 1. Synthesis Scheme 1. Synthesis routes for nitrogen-containing heterocyclic dialkyl dithiocarbamate derivatives: (**a**) Synthetic route of intermediate NaDBTC; (**b**) Synthetic routes of final products Py-2-DBDTC, PDM-DBDTC and BZT-DBDTC.

2. Experimental Section

2.1. Materials

n-Butylamine (99.0%), carbon disulfide (99.0%), 2-(Bromomethyl) pyridine hydrobromide (96.0%), and 2-(Chloromethyl) benzothiazole (98.0%) were all obtained from Saien Chemical Technology Co., Ltd. (Shanghai, China). Tetrahydrofuran (99.9%) was purchased from China National Medicines Chemical Reagent Co., Ltd. (Shanghai, China). 2,6-Bis(bromomethyl)pyridine (98.0%) and sodium hydroxide (98.0%) were supplied by Shanghai Titan Scientific Co., Ltd.(Shanghai, China). The base oil PAO4 was sourced from ExxonMobil Corporation. Commercially available dibutyl dithiocarbamate (DBDTC) was utilized as a comparative lubricant additive in this study. All reagents were of commercial grade and used without further purification.

2.2. Synthesis

2.2.1. Synthesis of Pyridin-2-ylmethyl dibutyl dithiocarbamate (Py-2-DBDTC)

In a 500 mL round-bottomed flask, 2.714 g (0.021 mol) of di-n-butylamine and 30 mL of tetrahydrofuran solution were added. Meanwhile, 20 mL of aqueous sodium hydroxide solution containing 0.840 g (0.021 mol) of sodium hydroxide was added, and the mixture was placed in an ice-water bath at 0 °C. A solution of 1.60 g (0.021 mol) of carbon disulfide dissolved in 10 mL of tetrahydrofuran was added dropwise, with continuous stirring sustained in the ice bath for 0.5 h. Then, the ice bath was removed, the temperature was raised to 25 °C, and the reaction was allowed to proceed for another 6 h. Through the substitution reaction, the intermediate butyl dithiocarbamate (NaDBTC) was obtained, and the solution exhibited a yellow-green color.

Subsequently, the solution containing the intermediate was placed in a 0 °C ice bath and 20 mL of tetrahydrofuran solution containing 2.53 g (0.01 mol) of 2-(bromomethyl)pyridine hydrobromide was added dropwise. The mixture was stirred in the ice bath for 0.5 h, then heated to 85 °C, and stirred for 18 h until the reaction was complete. The reaction was quenched with water. Add 200 mL of water and 100 mL of ethyl acetate to the solution. Separate the organic and aqueous phases, and then dry over anhydrous sodium sulfate. Finally, remove the solvent by distillation to obtain the crude product. Column chromatography (elution: PE/EA = 8/2) yielded a deep-green liquid pure product (2.93 g, 73.43%). The NMR and mass spectrometry data are detailed in Supporting Information S1. NMR spectra are provided in Figure S1(a2,a3). Characteristic molecular ion peaks are shown in Figure S2a.

2.2.2. Synthesis of 2,6-Bis (dibutyl dithiocarbamoyl methyl) pyridine (PDM-DBDTC)

An equivalent amount of the intermediate (NaDBTC) was prepared in a 500 mL round-bottom flask using the method described in Section 2.2.1. Under an ice bath maintained at 0 °C, 20 mL of tetrahydrofuran solution containing 2.65 g (0.01 mol) of 2,6-bis(bromomethyl)pyridine was added dropwise to the intermediate solution. Stirring was maintained in the ice bath for 0.5 h, after which the temperature was raised to 85 °C and reflux was carried out for 24 h. Upon completion of the reaction, it was quenched with water. After being washed with water, the organic phase was extracted with ethyl acetate solution. The crude product was obtained by drying with anhydrous sodium sulfate and removing the solvent via distillation. Purification by column chromatography (elution: PE/EA = 9/1) was performed, yielding the pure product as a yellow liquid (3.26 g, 65.37%). The NMR and mass spectrometry data are detailed in Supporting Information S1. NMR spectra are provided in Figure S1(b2,b3). Characteristic molecular ion peaks are shown in Figure S2b.

2.2.3. Synthesis of Benzothiazol-2-ylmethyl dibutyl dithiocarbamate (BZT-DBDTC)

The final product BZT-DBDTC was synthesized via a substitution reaction between 1.84 g (0.01 mol) of 2-(chloromethyl) benzothiazole and 2.27 g (0.01 mol) of the intermediate (NaDBTC), employing a methodology analogous to that for PDM-DBDTC and Py-2-DBDTC. The yield was 74.70%. The product was a dark-brown liquid. The NMR and mass spectrometry data are detailed in Supporting Information S1. NMR spectra are provided in Figure S1(c2,c3). Characteristic molecular ion peaks are shown in Figure S2c.

2.3. Structural Analysis of the Synthesized Compounds

Multiple analytical methods were employed to comprehensively characterize the structures of the compounds. The specific experimental procedures are as follows: Fourier-Transform Infrared Spectroscopy (FT-IR, PerkinElmer Frontier) was used to an-

alyze the compounds and functional group structures within the wavenumber range of 500–4000 cm^{-1}. ^{1}H NMR and ^{13}C NMR of the compounds were acquired at 600 MHz and 150 MHz, respectively, using a nuclear magnetic resonance spectrometer (AVANCE HD, Bruker, Billerica, MA, USA). The relative molecular masses of the compounds were determined using a mass spectrometer (MS6230–TOF, Agilent, Santa Clara, CA, USA).

2.4. Thermal Stability, Oxidation Stability, and Copper Strip Corrosion Measurement

The thermal stability of the three additives was evaluated using thermogravimetric analysis (TGA 55, TA Instruments, New Castle, DE, USA). Test conditions comprised a nitrogen atmosphere, an initial temperature of 40 °C, a heating rate of 10 °C/min to 500 °C, and a 10 min dwell at 500 °C. The initial oxidation temperature was measured using a Swiss Mettler-Toledo PDSC instrument (Greifensee, Switzerland) to characterize the samples' oxidative stability. The initial oxidation temperature was determined according to ASTM E2009-08 (2014) [28]. Test samples were prepared by blending each additive into PAO4 base oil at concentration ratios of 0.1 wt.%, 0.3 wt.%, 0.5 wt.%, 1.0 wt.%, and 2.0 wt.%. A 3.3 mg oil sample was placed in a sample pan and heated at a rate of 10 °C/min under an oxygen pressure of 3.5 MPa and flow rate of 50 mL/min until oxidative exothermic release occurred. The initial oxidation temperature was determined as the intersection point of the baseline extrapolation line and the tangent line at the maximum oxidative peak rate. According to the standard GB/T 5096-2017 [29], the polished copper strips were immersed in oil samples containing different concentrations of additives and maintained at 100 °C for three hours to complete the corrosion tests on non-ferrous metals for the three synthesized compounds and the commercial additive (DBDTC). The results are shown in Figure S3 and Table S1.

2.5. Tribological Testing

The tribological experiments employed an MS-10A four-ball friction and wear tester manufactured by Xiamen Tianji Co., Ltd. (Fujian, China). to assess the anti-wear, friction-reducing, and extreme-pressure properties of oil samples under point-to-point mode. The test balls were Grade 2 standard balls (AISI-52100) produced by Falex, with a diameter of 12.7 mm, material GCr15, and hardness of 59–61 HRC. The extreme-pressure performance of the oil samples was evaluated in accordance with GB/T 3142—2019 [30], which is technically comparable to ASTM D2783 [31] in terms of test principles and evaluation criteria. The maximum load without seizure (P_B) was measured at a rotational speed of 1450 r/min, a test temperature of 25 °C ± 5 °C, and a test duration of 10 s. Anti-wear performance was evaluated according to standard method NB/SH/T 0189—2017 [32] at 75 °C, with load levels of 196 N, 294 N, and 392 N, rotational speed of 1200 r/min, the experiment being repeated twice, and duration of 60 min.

Per Aachard's wear law [33], the wear rate is calculated as follows:

$$K = \frac{V}{FL} \tag{1}$$

where V denotes the wear volume (μm^3), F represents the normal load (N), and L indicates the sliding distance (mm). This equation facilitates the comparison of wear rates among samples under specific experimental conditions, thereby aiding in the evaluation of the anti-wear properties of various additives.

To evaluate the tribological properties of the synthesized compounds over a wide temperature range, linear reciprocating friction and wear tests were conducted using a multifunctional tribometer (Bruker UMT-Tribolab). The experimental parameters were optimized based on the ASTM G133 [34] standard and the practical service conditions of

the compounds. During testing, an 8 mm diameter AISI-52100 steel ball was subjected to a 5 N (initial contact pressure 900 MPa) normal load and reciprocated at a frequency of 1 Hz with a 10 mm stroke on an AISI-52100 steel base plate. Experiments were conducted under variable temperature conditions at 25 °C, 75 °C, 100 °C, and 150 °C. Prior to testing, both the substrate and steel balls underwent ultrasonic cleaning with petroleum ether and ethanol to remove surface impurities. To ensure the reliability of the average coefficient of friction, at least two replicate tests were conducted at each test temperature.

The surface morphology of the steel balls was characterized using optical microscopy, a non-contact optical 3D surface profiler (ContourGT-K, Bruker, Ettlingen, Germany), and scanning electron microscopy (SEM; ZEISS GeminiSEM 300, Oberkochen, Germany). Furthermore, the elemental composition and chemical properties of the friction surfaces were analyzed by the EDS surface energy spectrum, Raman spectroscopy (Horiba LabRAM HR Evolution, Kyoto, Japan), X-ray photoelectron spectroscopy (XPS; Thermo Scientific K-Alpha, Waltham, MA, USA), and time-of-flight secondary-ion mass spectrometry (ToF-SIMS). All the data plotting in the text was done using the software Origin 2025b.

3. Results

3.1. Structural Characterization of Multifunctional Nitrogen-Containing Heterocyclic Alkyl Thioamides

Figure 1 displays the FT-IR spectra of the three synthetic products Py-2-DBDTC, PDM-DBDTC, and BZT-DBDTC. Table 1 lists the infrared absorption peak information corresponding to each functional group in the three compounds. In Figure 1a, the peaks near 2952.39 cm^{-1} and 2882.75 cm^{-1} correspond to the C-H stretching vibrations of the $–CH_3$ and $–CH_2$ groups, respectively. The absorption peak near 1568.73 cm^{-1} corresponds to the stretching vibration of C=C or C=N bonds, indicating the presence of the central pyridine aromatic ring. The absorption peaks at 1460.12 cm^{-1} and 1390.33 cm^{-1} represent the bending vibrations of the $–CH_2$ and $–CH_3$ groups, respectively; the absorption peak near 1234.50 cm^{-1} corresponds to the C–N stretching vibration of the tertiary amino group; the peak near 1198.08 cm^{-1} represents C–S stretching vibrations; and peaks near 874.26 cm^{-1} and 730.09 cm^{-1} correspond to out-of-plane bending vibrations of C–H bonds within the pyridine ring. This supports the 1,2,6-trisubstituted structure of the pyridine ring and confirms the successful synthesis of Py-2-DBDTC. Comparing the molecular structures of Py-2-DBDTC and PDM-DBDTC reveals identical functional groups. Figure 1b and Table 1 confirm the successful synthesis of PDM-DBDTC.

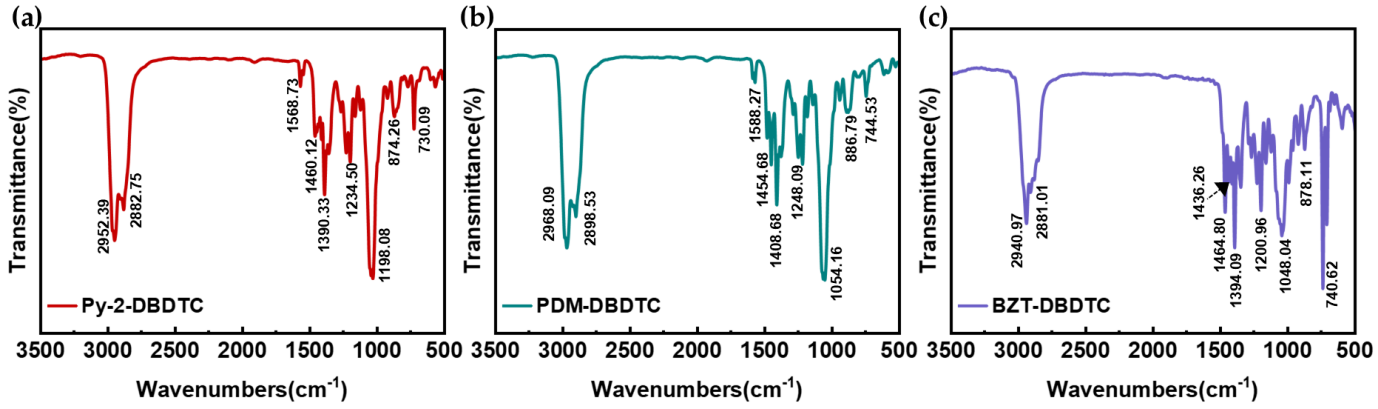


Figure 1. The FT-IR spectra of (**a**) Py-2-DBDTC, (**b**) PDM-DBDTC, and (**c**) BZT-DBDTC.

Table 1. Infrared data for Py-2-DBDTC, PDM-DBDTC, and BZT-DBDTC and their corresponding functional groups.

Functional	Py-2-DBDTC (cm^{-1})	PDM-DBDTC (cm^{-1})	BZT-DBDTC (cm^{-1})
$-CH_3$, $-CH_2$	2952.39, 2882.75	2968.09, 2898.53	2952.39, 2882.75
C=C, C=N	1568.73	1588.27	1436.26
$-CH_2$, $-CH_3$	1460.12, 1390.33	1454.68, 1408.68	1436.26, 1394.09
C-N	1234.50	1248.09	1200.96
C-S	1198.08	1054.16	1048.04
aromatic ring (-CH)	874.26, 730.09	886.79, 744.53	878.11, 740.62

In the infrared spectrum of Figure 1c, absorption peaks near 2940.97 cm^{-1} and 2881.01 cm^{-1} correspond to the C-H stretching vibrations of the $-CH_3$ and $-CH_2$ groups, respectively; the absorption peak near 1464.80 cm^{-1} corresponds to the stretching vibration of C=C or C=N bonds; peaks near 1436.26 cm^{-1} and 1394.09 cm^{-1} correspond to the bending vibrations of $-CH_2$ and $-CH_3$ groups; the absorption peak at 1200.96 cm^{-1} represents the C-N stretching vibration of the tertiary amino group; the absorption peak near 1048.04 cm^{-1} corresponds to C-S stretching vibrations; and peaks near 878.11 cm^{-1} and 740.62 cm^{-1} are attributed to out-of-plane C-H bending vibrations of the aromatic ring, confirming the ortho-substituted structure of the benzothiazole ring. In summary, BZT-DBDTC has also been successfully synthesized.

3.2. Thermal Stability and Oxidation Stability Performance

Under complex and variable friction conditions, ensuring the sustained efficacy of multifunctional lubricant additives is paramount to the additives themselves. Among these, TGA thermal decomposition testing and PDSC initial oxidation temperature testing provide straightforward and intuitive evaluations of an additive's thermal decomposition stability and thermal oxidation stability. As illustrated in Figure 2a, the initial decomposition temperatures of all three additives exceeded 200 °C. Additive PDM-DBDTC demonstrated the most outstanding performance with an initial decomposition temperature of 283.42 °C. BZT-DBDTC followed with an initial decomposition temperature of 260.10 °C. Py-2-DBDTC exhibited the lowest initial decomposition temperature among the three additives.

The antioxidant performance of the three additives was evaluated by measuring their initial oxidation temperature using pressurized differential scanning calorimetry (PDSC) at different concentrations. As shown in Figure 2b, the initial oxidation temperature of all three additives continued to rise with increasing concentration and reached its respective maximum at an additive concentration of 3.0 wt.%. Specifically, the oil samples containing PDM-DBDTC and BZT-DBDTC achieved initial oxidation temperatures of 214.19 °C and 214.69 °C, respectively, representing an increase of approximately 16.9 °C compared to the base oil. In contrast, the oil sample with 3.0 wt.% Py-2-DBDTC exhibited an initial oxidation temperature of 206.33 °C, indicating significantly lower oxidation stability than the former two additives. In summary, the antioxidant performance of the oil samples showed a positive correlation with additive concentration. Organic sulfur compounds, as typical secondary antioxidants, exert their antioxidative effect by decomposing peroxides via sulfur-containing functional groups [35,36]. Consequently, a higher additive concentration corresponds to a greater number of sulfur-containing functional groups, leading to more rapid decomposition of peroxides and thereby enhancing antioxidant performance.

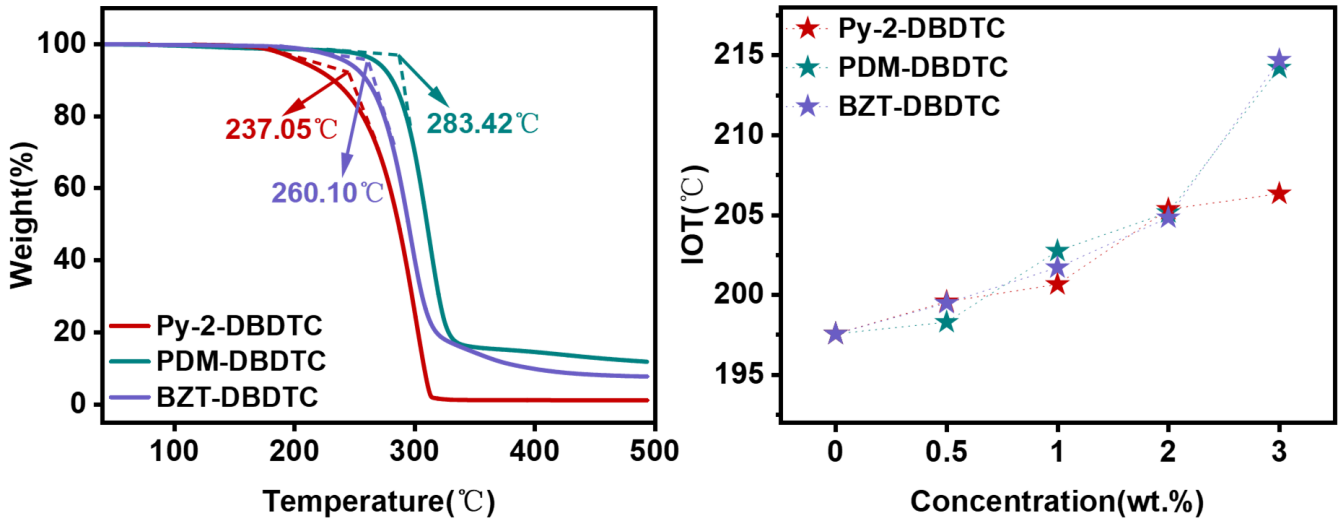


Figure 2. (**a**) TGA curves of Py-2-DBDTC, PDM-DBDTC, and BZT-DBDTC; (**b**) initial oxidation temperature of oils with different concentrations.

3.3. Analysis of Tribological Properties

3.3.1. Frictional Behavior Under Point-to-Point Rotational Friction Conditions

The anti-wear performance of additives was evaluated using a four-ball friction and wear tester under a point-to-point rotational friction mode, with experimental results shown in Figure 3a. It can be observed that under pure base oil conditions, the wear scar diameter measured 0.808 mm. In contrast, the wear scar diameters for lubricants with additives at every concentration were smaller than that of the base oil. As additive concentration increased, the wear scar diameters of the three oil samples exhibited a trend of initially decreasing before subsequently increasing. At an additive concentration of 0.1 wt.%, all oil samples achieved their minimum wear scar diameters. The oil sample containing PDM-DBDTC exhibited a wear scar diameter of 0.406 mm, representing a 49.75% reduction compared to the base oil and demonstrating marginally superior anti-wear performance compared to Py-2-DBDTC (0.443 mm) and BZT-DBDTC (0.440 mm) oils. Further increasing the additive concentration caused a gradual increase in the wear scar diameters, reaching their maximum values at a concentration of 2.0 wt.%. Based on these results, it can be inferred that at the optimal concentration, the additive molecules decompose during the friction process, and the S–S bonds in their structure break and undergo chemical reactions with the metal to form a protective tribochemical film, thereby exerting an anti-wear effect [37]. However, a further increase in additive concentration leads to amplified corrosive effects from the active sulfur elements in the molecular structure, which can cause corrosion or embrittlement of the metal surface [38]. Consequently, the anti-wear performance is overshadowed by this corrosive inhibition, resulting in an increase in the wear scar diameter. As shown in Figure S3, the synthesized compounds and the commercial additive exhibit comparable levels of corrosion on copper strips. When the concentration is below 0.5 wt.%, all samples cause relatively mild corrosion to the copper strips. As the concentration increases further, their corrosive behavior changes significantly. When the concentration reaches 2.0 wt.%, the corrosion level caused by each type of additive on the copper strips reaches the highest grade.

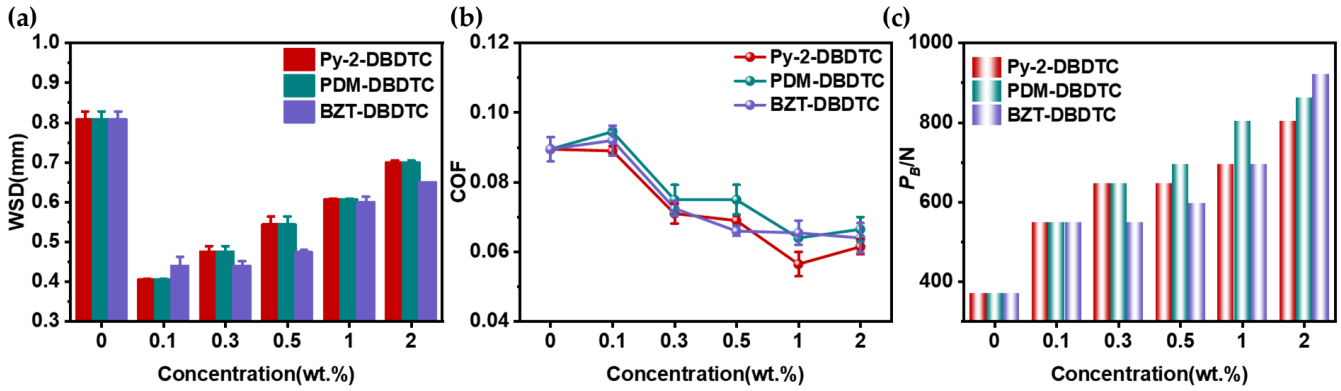


Figure 3. Tribological performance of Py-2-DBDTC, PDM-DBDTC, and BZT-DBDTC at different concentrations: (**a**) average wear spot diameter; (**b**) average coefficient of friction; (**c**) load-carrying capacity (P_B value).

In the point-to-point rotational friction mode, the influence of additive concentration on friction-reducing performance is illustrated in Figure 3b. At a 0.1 wt.% additive concentration, no significant friction-reducing effect was observed compared to the base oil. At a concentration of 0.3 wt.%, the friction coefficients of all three additive-containing oil samples exhibited a significant reduction compared to the base oil. Furthermore, each additive achieved its optimal anti-friction effect at a concentration of 1.0 wt.%. Beyond this concentration, the friction coefficient showed no noticeable change, indicating that the anti-friction effect stabilized. Regarding the above phenomenon, it may be attributed to the fact that at relatively low additive concentrations, the adsorption of additive molecules on the substrate surface involves competitive interactions, preventing stable adsorption and thus resulting in an inhibition of friction reduction for the oil samples at this concentration. As the concentration gradually increases, the additives can adsorb stably at the friction interface and undergo tribochemical reactions with the substrate to form a tribofilm, allowing the friction-reducing effects of the additives to become significantly pronounced.

The extreme-pressure properties of additives serve as a key factor in the load-carrying capacity of lubricants during friction processes, effectively preventing adhesion and wear between metal components under severe extreme-pressure conditions. To further investigate the influence of additive concentration on extreme-pressure performance, a four-ball test machine was employed. As shown in Figure 3c, all three additives significantly enhanced the extreme-pressure performance of the base oil across all concentrations tested. Extreme-pressure performance exhibits a close and positive correlation with additive concentration. When the concentration of all three additives reached a maximum of 2.0 wt.%, each oil sample attained its maximum no-seizing load (PB). Notably, the P_B value of the oil sample containing BZT-DBDTC reached 921.2 N, representing a 147.37% improvement over the base oil's extreme-pressure performance, while the PB values for the PDM-DBDTC- and Py-2-DBDTC-containing oils reached 862.4 N and 803.6 N, respectively. All three additives demonstrated outstanding extreme-pressure performance. Notably, unlike the anti-wear behavior patterns of the additives, extreme-pressure performance consistently exhibited linear growth with increasing concentration. This is primarily related to the strength of the C-S bond within the additive structure and the sulfur content [39,40]. As the load continues to increase, the C-S bonds within the molecular structure begin to break, forming a solid sulfide iron film. A higher additive content further facilitates this process, inhibiting metal adhesion and seizure, thereby effectively utilizing the additive's extreme-pressure properties [41].

Subsequently, a typical commercial ashless additive, dibutyl dithiocarbamate (DBDTC), was selected for comparative evaluation of anti-wear, friction-reducing, and extreme-pressure performance under identical conditions with the synthesized compounds. The results are presented in Figure S4. It can be observed that the wear scar diameters of the three synthesized compounds reach their minimum values at a concentration of 0.1 wt.%, with their optimal wear scar diameters being smaller than that of the commercial additive at 0.5 wt.%. Comparative data on friction coefficients reveal that, at 0.3 wt.%, the three synthesized compounds exhibit a significant reduction in friction coefficient compared to the base oil, whereas the commercial additive demonstrates friction-reducing performance only when its concentration is increased to 1.0 wt.%. Extreme-pressure test data indicate that the extreme-pressure performance of both the synthesized compounds and the commercial additive improves with increasing concentration, with all four additives exhibiting similar extreme-pressure properties.

3.3.2. Frictional Behavior Under Ball-on-Flat Reciprocating Sliding Conditions

To comprehensively investigate the tribological properties of multifunctional additives under varying operating conditions, reciprocating friction tests were conducted on each additive using a UMT friction tester. Optimal concentration screening was performed at 75 °C, as illustrated in Figure 4. Overall, all three additives demonstrated significantly reduced friction compared to the base oil in reciprocating mode, exhibiting a close correlation with concentration. At 0.1 wt.%, the friction curves of the three additive-containing oil samples did not flatten, with only a modest decrease in the coefficient of friction. However, when the concentration was increased to 0.3 wt.%, the anti-friction effects of all three additives became markedly pronounced, with friction curves flattening and friction coefficients decreasing substantially. Among these, the PDM-DBDTC and Py-2-DBDTC oil samples achieved optimal anti-friction performance, exhibiting average friction coefficient reductions of 45.54% and 43.60%, respectively, compared to the base oil. Beyond 0.3 wt.%, both samples showed a slight increase in friction coefficient. The average friction coefficient of the BZT-DBDTC oil sample, however, decreased continuously with increasing concentration, achieving optimal anti-friction performance at 2.0 wt.%. The average friction coefficient was reduced by approximately 46.10% compared to the base oil.

Figure 4e,f present optical characterization of wear patterns on friction pairs using the base oil sample and various oil samples at 0.3 wt.% concentration. The base oil exhibited severe grooves and severe wear scarring. In contrast, the surfaces of wear scars from friction involving the three additive-containing oil samples appeared smooth and flat, with no discernible grooves. This demonstrates that all three additives deliver equally excellent wear resistance performance under reciprocating mode.

3.3.3. The Effect of Temperature on Tribological Properties

To address complex and variable friction conditions, tribological testing was conducted on three oil samples containing 0.3 wt.% additives across a broad temperature range of 25–150 °C, investigating the influence of temperature on the additives' friction-reducing properties. As shown in Figure 5a, all three additives exhibited superior anti-friction performance below 75 °C, with friction coefficients significantly lower than the base oil. This indicates that during the friction process conditions, the additives facilitate the formation of physically adsorbed films and friction chemical reaction films, thereby delivering anti-friction effects. Above 100 °C, both the anti-friction performance and repeatability of the base oil deteriorated markedly. The friction coefficients of all additives generally increased but remained significantly lower than the base oil, maintaining superior anti-friction performance. As shown in Figure 5a, the average friction coefficients of Py-2-DBDTC,

PDM-DBDTC, and BZT-DBDTC oil samples at 150 °C decreased by 39.19%, 51.59%, and 54.13%, respectively. Notably, the friction-reducing effects of PDM-DBDTC and BZT-DBDTC oil samples showed no discernible difference above 100 °C, with their friction curves remaining nearly identical. Conversely, the friction-reducing efficacy of Py-2-DBDTC oil samples markedly diminished, with its friction curve distinctly higher than the other two. By comparing the molecular structures of Py-2-DBDTC and PDM-DBDTC, it can be observed that PDM-DBDTC contains a significantly greater number of dithiocarbamate groups, the key functional groups responsible for tribological performance, than Py-2-DBDTC. This structural difference facilitates a more effective formation of tribochemical films in PDM-DBDTC. Similarly, comparing the molecular structures of BZT-DBDTC and Py-2-DBDTC reveals that the benzothiazole ring in BZT-DBDTC exhibits stronger adsorption capability, which accelerates the participation of additive molecules in the formation of chemical reaction films during the friction process. It is hypothesized that these factors contribute to the superior friction-reducing performance of PDM-DBDTC and BZT-DBDTC compared to Py-2-DBDTC.

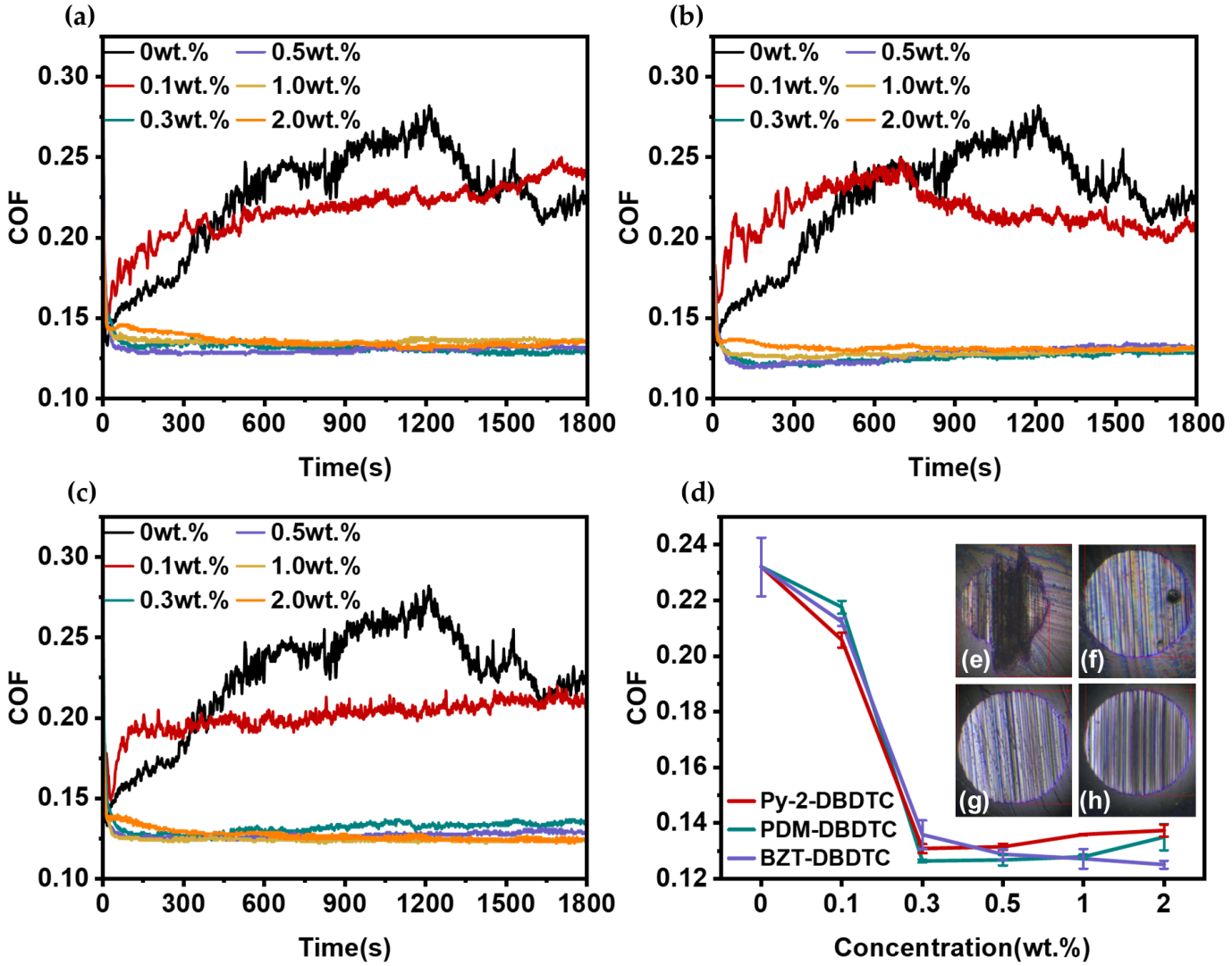


Figure 4. Friction coefficient of (**a**) Py-2-DBDTC, (**b**) PDM-DBDTC, and (**c**) BZT-DBDTC at different concentrations at 75 °C; (**d**) average coefficient of friction for Py-2-DBDTC, PDM-DBDTC, and BZT-DBDTC at various concentrations; (**e**–h) Wear scar morphologies of steel balls sequentially lubricated with PAO4, 0.3 wt.% Py-2-DBDTC, 0.3 wt.% PDM-DBDTC and 0.3 wt.% BZT-DBDTC.

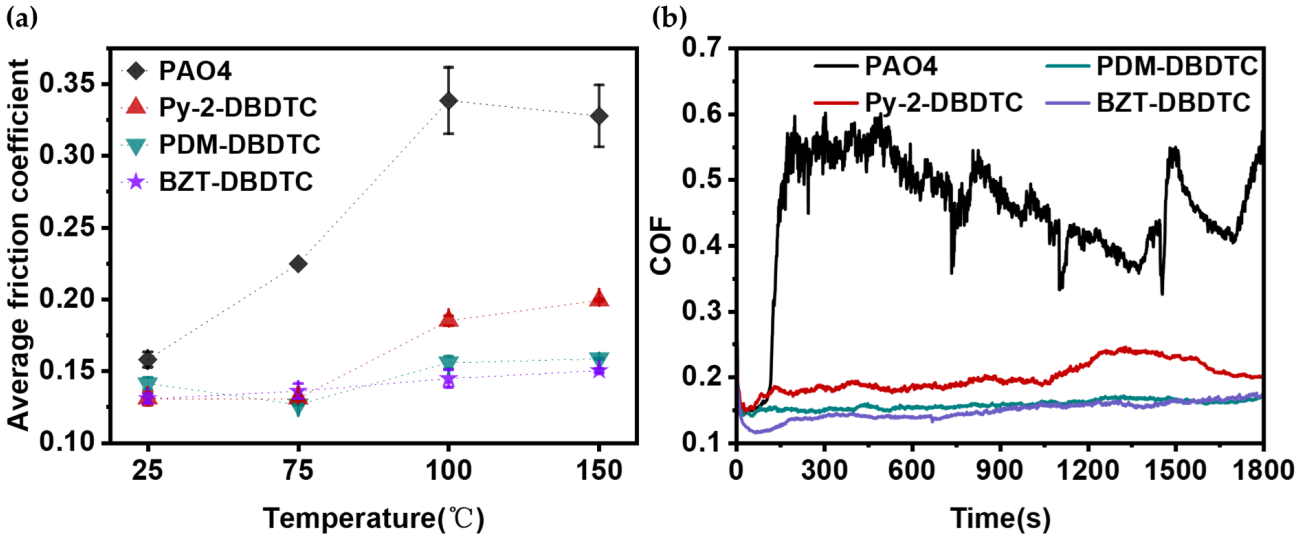


Figure 5. (**a**) Average coefficient of friction at 25–150 °C; (**b**) friction curves of PAO4, 0.3 wt.% Py-2-DBDTC, 0.3 wt.% PDM-DBDTC, and 0.3 wt.% BZT-DBDTC at 150 °C.

3.4. Analysis of Worn Surfaces

3.4.1. Characterization of Abrasion Scratch Morphology

To further validate the lubrication performance and mechanisms of the three additives—Py-2-DBDTC, PDM-DBDTC, and BZT-DBDTC—the surface morphology of the wear scars on steel balls after prolonged four-ball tests was analyzed using white light interferometry and scanning electron microscopy (SEM). The analysis was conducted on the base oil and the three oil samples containing 0.3 wt.% additive, as shown in Figure 6 and Table 2. Results indicate that under base oil lubrication conditions, the wear scar depth reached 29.16 μm with a width of 0.89 mm, exhibiting the highest wear rate (K_W: 1.538 × 10^{-5} $\mu m^3/(N \cdot mm)$). Images reveal severe grooving in the base oil wear scar, exhibiting an extremely rough morphology with a limited lubricating effect, failing to effectively reduce surface wear. In contrast, the wear rates on the steel ball surface were significantly reduced after lubrication with the three additive-containing oil samples. Following lubrication with PDM-DBDTC, the wear scar depth reached 7.19 μm and width 0.49 mm, with the lowest wear rate among the three additives (K_W: 4.827 × 10^{-6} $\mu m^3/(N \cdot mm)$). Py-2-DBDTC and BZT-DBDTC also demonstrated excellent lubricating properties, reducing wear rates by 62.10% and 58.34%, respectively, compared to the base oil. Electron microscope images reveal that the abrasion marks lubricated by all three additives exhibit no pronounced grooves, with relatively smooth surfaces. This indicates that the additives effectively reduce wear while improving surface smoothness, thereby delivering anti-wear and friction-reducing lubrication effects.

Table 2. Steel ball wear rates from four-ball tests of PAO4, 0.3 wt.% Py-2-DBDTC, 0.3 wt.% PDM-DBDTC, and 0.3 wt.% BZT-DBDTC.

Samples	V (μm^3)	F (N)	L (mm)	Kw ($\mu m^3/(N \cdot mm)$)
PAO4	4.589	196	325,058	1.538×10^{-5}
0.3 wt.% Py-2-DBDTC	1.895	196	325,058	5.829×10^{-6}
0.3 wt.%PDM-DBDTC	1.569	196	325,058	4.827×10^{-6}
0.3 wt.% BZT-DBDTC	2.083	196	325,058	6.408×10^{-6}

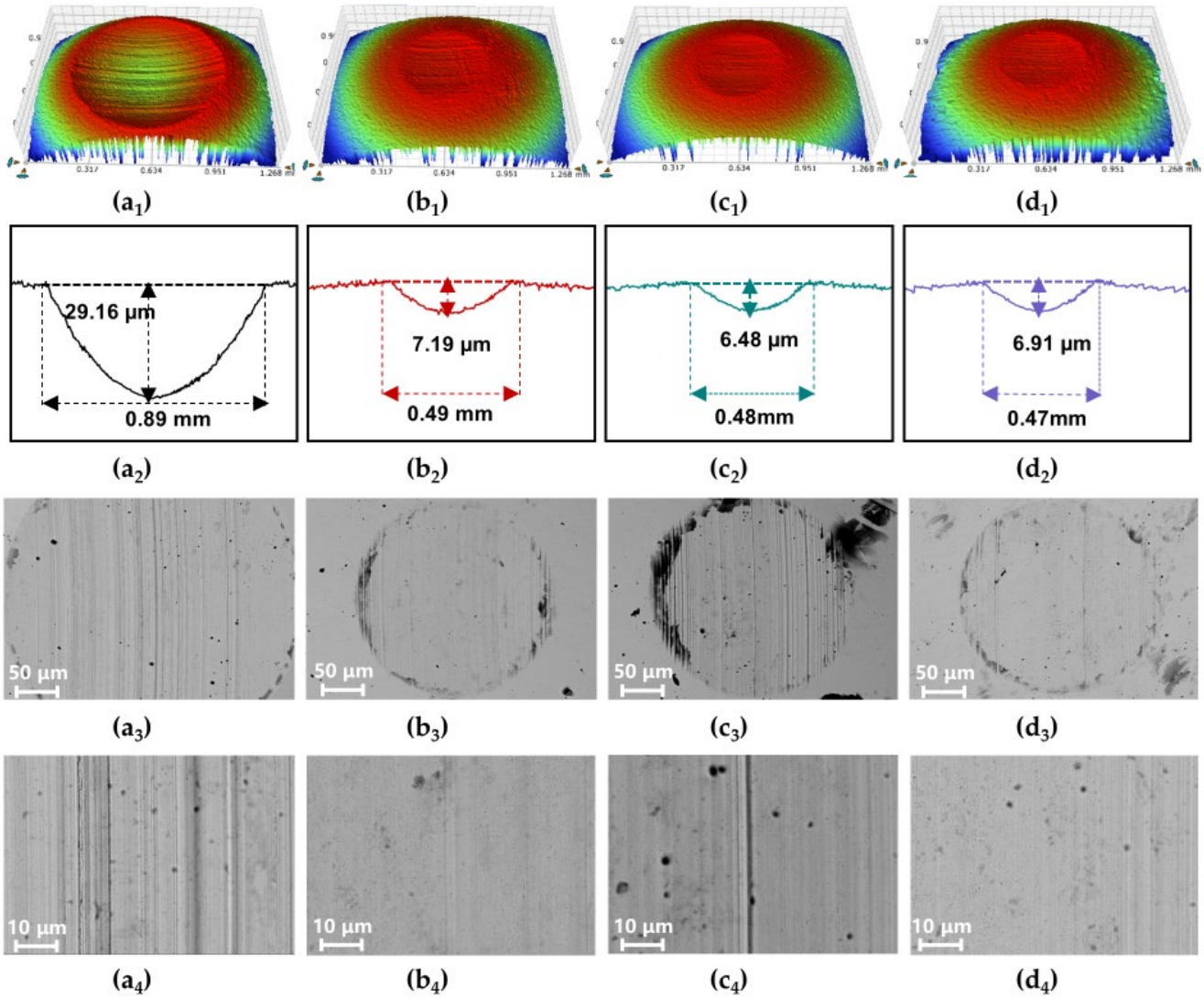


Figure 6. Surface wear and morphology of steel balls after the four-ball friction tests: (**a$_1$**–**a$_4$**) PAO4; (**b$_1$**–**b$_4$**) 0.3 wt.% Py-2-DBDTC; (**c$_1$**–**c$_4$**) 0.3 wt.% PDM-DBDTC; (**d$_1$**–**d$_4$**) 0.3 wt.% BZT-DBDTC.

3.4.2. Elemental Analysis of the Worn Steel Ball Surface

Energy-Dispersive Spectroscopy (EDS) analysis was performed to characterize the distribution of C, O, S, Fe, and N elements on the worn surfaces. As shown in Figure 7, no significant nitrogen deposition was detected on the surfaces lubricated with the three oil samples containing 0.3 wt.% additives, which may be attributed to the low sensitivity of EDS. Significant carbon enrichment was observed on wear scars from both the base oil and additive-containing oils, indicating the formation of carbon-based protective films during friction that reduce direct metal contact and lower friction and wear. The observed oxygen enrichment is hypothesized to result from reactions between freshly exposed metal surfaces and atmospheric oxygen, forming iron oxides. Additionally, significant sulfur enrichment was detected at wear scar sites lubricated with additive-containing oils, suggesting that the additives undergo tribochemical reactions with the metal surface to form a protective film. This tribochemical film effectively isolates friction pairs, reduces the friction coefficient, and significantly enhances anti-wear performance.

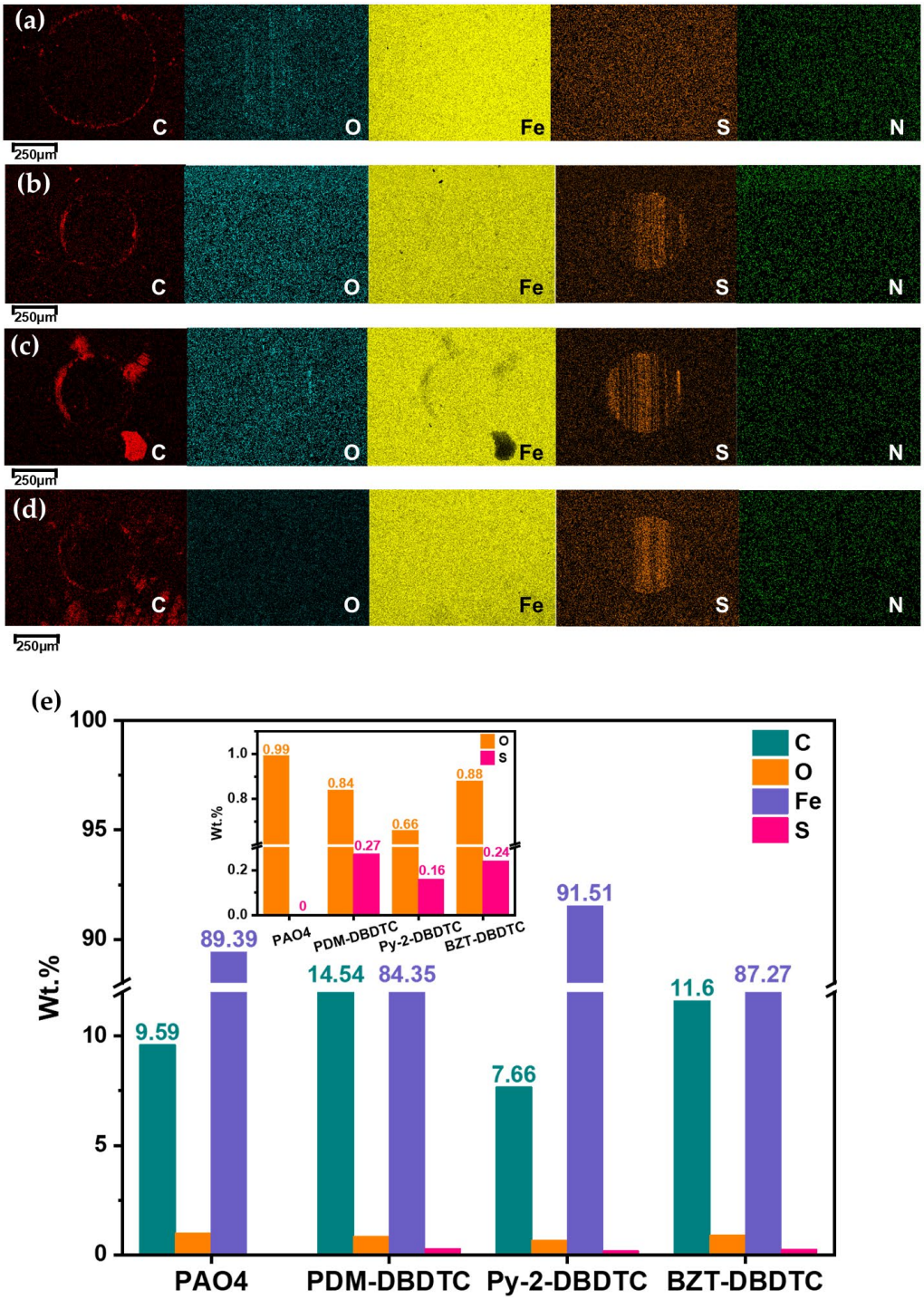


Figure 7. EDS mapping of steel wear scars after the four-ball friction tests: (**a**) PAO4, (**b**) 0.3 wt.% Py-2-DBDTC, (**c**) 0.3 wt.% PDM-DBDTC, (**d**) 0.3 wt.% BZT-DBDTC. (**e**) EDS elemental composition analysis of friction surfaces.

3.4.3. Surface Scratch Raman and XPS Analysis

Raman spectroscopy analysis of the worn surface was conducted to examine the composition of the protective layer formed on the metal surface, as shown in Figure 8a. Within the spectrum, peaks near 366 cm^{-1} and 668 cm^{-1} correspond to characteristic features of Fe_2O_3 and Fe_3O_4, respectively [42]. The D peak near 1396 cm^{-1} reflects disordered carbon structures within carbon-based materials, while the G peak at 1574 cm^{-1} originates from in-plane vibrations of sp^2-hybridized carbon atoms [9,10]. The presence of both D and G

peaks indicates the existence of carbon-based materials on the metal surface. The peak near 2910 cm^{-1} represents −CHx (x = 1/2/3) groups within alkyl chains [43]. Comparing the Raman spectra of the base oil and additive in Figure 8a reveals an extremely weak signal for the iron oxide peak in the base oil. Combined with the three-dimensional morphology of the abrasion surface, this indicates severe plastic deformation of the base oil-lubricated surface during friction, suggesting possible delamination and peeling of the friction oxide layer. In contrast, the surface micro-scratch morphology lubricated by the three oil samples containing 0.3 wt.% additives showed no severe plastic deformation, with a relatively strong Fe_2O_3 peak signal. This indicates that the metal surface lubricated by additives can retain the friction oxide layer. Moreover, the simultaneous appearance of the D and G peaks in the Raman spectra effectively characterizes the structural features of the carbon film [39], indicating that the carbon film formed at the friction interface primarily consists of disordered carbon materials derived from sp^2-hybridized carbon structures [36,40]. Based on the comprehensive Raman data, it can be concluded that the wear scar surfaces lubricated by both the pure base oil and the additive-containing oil samples are mainly composed of amorphous carbon films and iron oxides.

To further investigate the lubrication mechanism, XPS characterization analysis was performed on the metal surface after friction, as shown in Figures 8 and S5. Figure 8b displays the C1s spectrum data of the friction surface. The peak at 284.8 eV corresponds to C-C/C-H bonds, while the peak near 287.6 eV corresponds to C-O or C-N bonds [44]. Figure 8c presents the Fe2p spectrum data. Peaks at 710.5 eV and 724.0 eV indicate the formation of Fe_2O_3, Fe_3O_4, and Fe(OOH) on the abraded surface. In the O1s spectrum, combined with the 710.5 eV peak in the Fe2p spectrum, the peak near 529.9 eV corresponds to iron oxides, while the peak at 531.7 eV corresponds to C-O bonds [45]. Figure 8e shows the N1s spectrum, revealing a C–N bond peak at 399.6 eV [46]. Figure 8f presents the S2p XPS spectrum, where the peak at 168.1 eV corresponds to SO_4^{2-}, while those near 163.1 eV and 162.0 eV correspond to S^{2-} [26]. Based on the combined results, it can be concluded that a thin film containing C, N, and O is formed on the friction surface. Furthermore, it can be inferred that the additive molecules preferentially adsorb onto the steel surface during the lubrication process. Subsequently, under friction, the additives decompose, and the active S elements—which play a key functional role—undergo chemical reactions with the metal surface. This leads to the formation of a lubricating film in the friction zone, composed of sulfides, inorganic sulfates, oxides, and related compounds.

3.4.4. Time-of-Flight Secondary-Ion Mass Spectrometry (ToF-SIMS) Analysis

To verify the above hypothesis, ToF-SIMS analysis was performed on the friction interfaces lubricated by the three types of oil samples containing 0.3 wt.% additives. The results are presented in Figure 9. The data reveal a series of hydrocarbon ion fragments, such as $C_2H_3^+$, $C_2H_5^+$, and $C_5H_7^+$, indicating the decomposition of hydrocarbon base oil into chain-scission molecules during friction. Simultaneously, the worn surfaces exhibit a substantial number of nitrogen- and sulfur-containing ion fragments, including NH_4^+, CN^-, SO_3^-, and SO_4^-, along with the presence of $FeOH^+$. These findings confirm that the active nitrogen (N) and sulfur (S) elements from the additive molecules participate in the formation of the surface tribofilm. Overall, the results demonstrate that the additive molecules effectively adsorb onto the metal surface. During high-speed and high-load friction, the dialkyl dithiocarbamate or benzothiazole groups in the additive molecules undergo cleavage of S–S or C–S bonds. The resulting active sulfur atoms then chemically react with the metal surface to form a protective film composed of sulfides, inorganic sulfates, oxides, and related compounds. It is the presence of this protective film that

prevents direct contact between the friction pairs, thereby significantly reducing friction and wear through enhanced tribological performance.

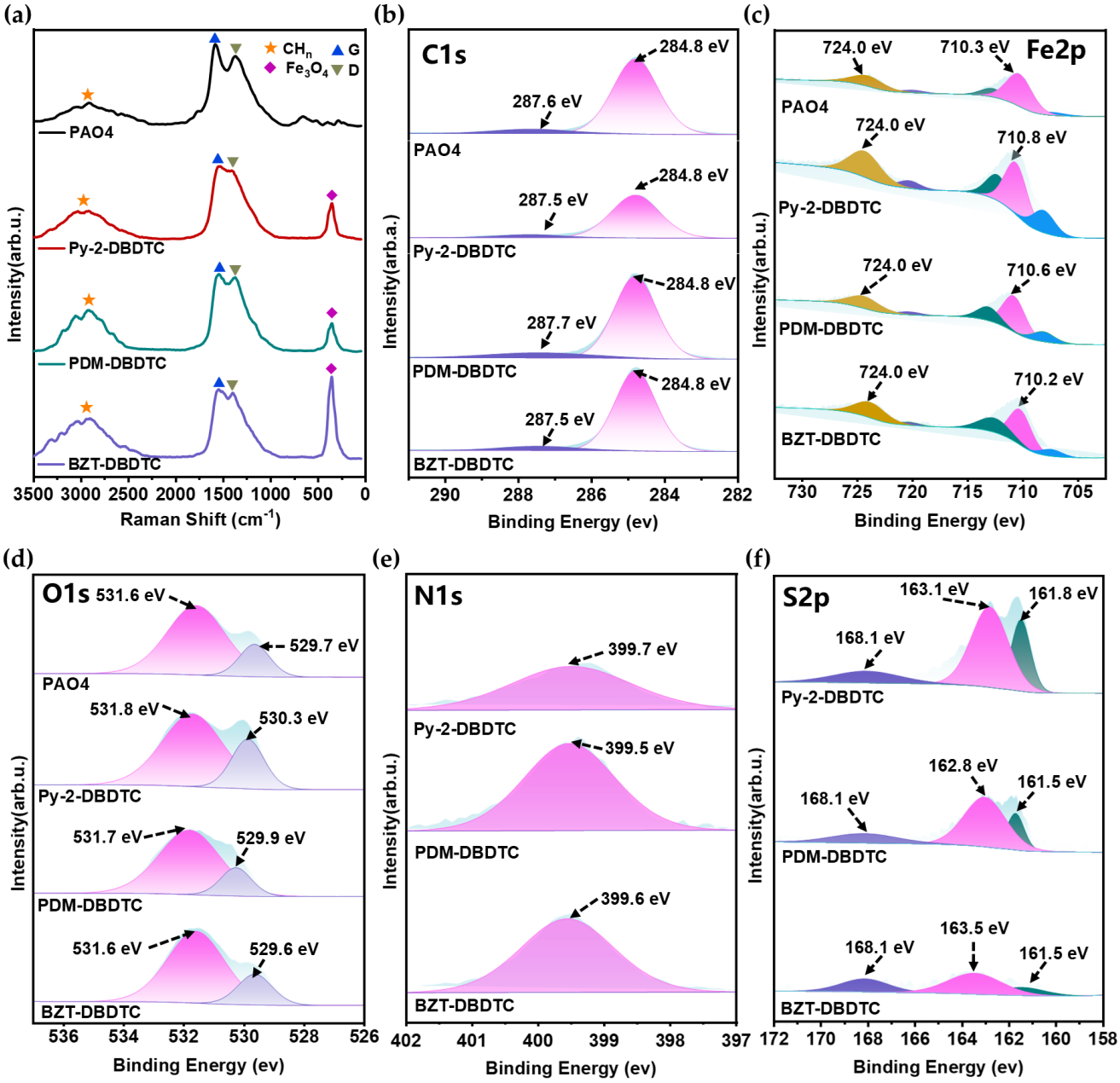


Figure 8. (**a**) Raman spectra of wear surface lubricated by PAO4, 0.3 wt.% Py-2-DBDTC, 0.3 wt.% PDM-DBDTC, and 0.3 wt.% BZT-DBDTC; comparison of XPS spectra of worn surfaces after lubrication with PAO4, 0.3 wt.% Py-2-DBDTC, 0.3 wt.% PDM-DBDTC, and 0.3 wt.% BZT-DBDTC: (**b**) C1s, (**c**) Fe2p, (**d**) O1s, (**e**) N1s, and (**f**) S2p.

3.5. Speculation on the Mechanism of Lubrication

Based on the aforementioned experiments and characterization of the worn surfaces, it can be hypothesized that the lubrication mechanism of nitrogen-containing heterocyclic alkyl dithiocarbamate derivatives is as illustrated in Figure 10. Firstly, the presence of nitrogen-containing heterocycles within the additive molecular structure increases adsorption sites, promoting the formation of coordination bonds between additive molecules and the metal surface, thereby accelerating the formation of the physical adsorption layer. As the friction process progresses, the adsorption layer may undergo desorption and decom-

position due to the harsh friction environment characterized by high temperatures and pressures. Consequently, the S-S and C-S bonds within the additive molecules break. The resulting active sulfur atoms then undergo tribochemical reactions with the metal substrate, forming a friction film composed of sulfide compounds and inorganic sulfates. This synergistic interaction between the adsorbed layer and the chemically reacted film enables the additive to sustain superior tribological performance during the friction process.

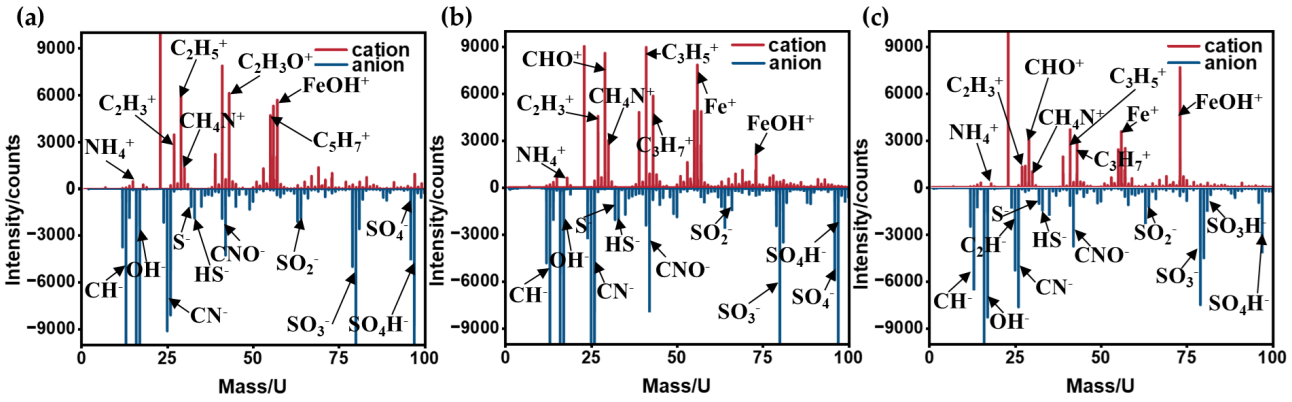


Figure 9. ToF-SIMS data of the wear surfaces lubricated by (**a**) 0.3 wt.% Py-2-DBDTC, (**b**) 0.3 wt.% PDM-DBDTC, and (**c**) 0.3 wt.% BZT-DBDTC.

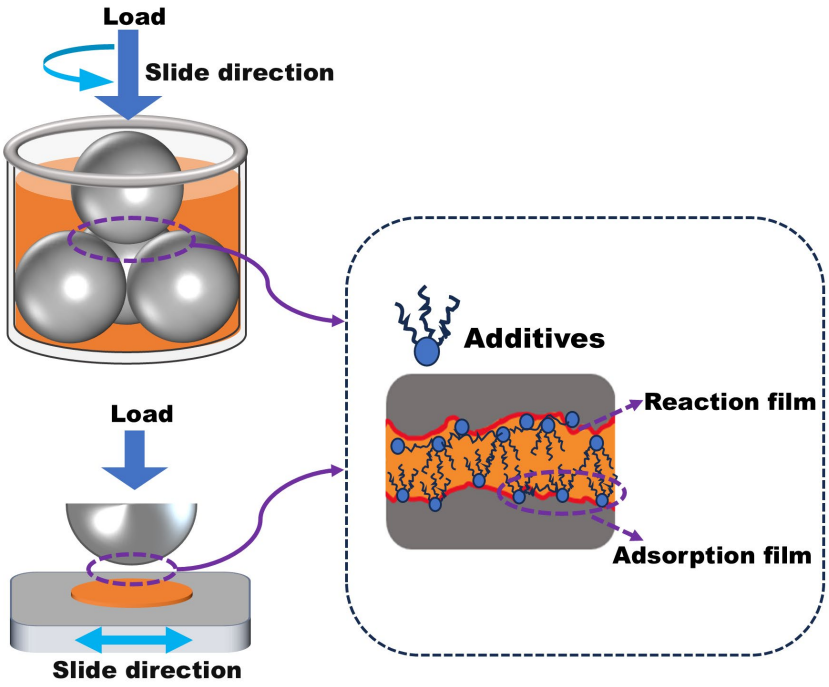


Figure 10. Friction mechanism diagram.

4. Conclusions

We have synthesized three novel nitrogen-containing heterocyclic alkyl dithiocarbamate derivatives as ashless, phosphorus-free multifunctional lubricant additives. This study also examined the tribological properties of the additives under various operating conditions and investigated the influence of structure on the molecular tribological performance of the additives. The principal conclusions are as follows:

Three nitrogen-containing heterocyclic dialkyl dithiocarbamate derivatives were synthesized via a simple and efficient method, with their structures confirmed by NMR, IR, and MS characterization techniques.

Thermogravimetric analysis indicated that the synthesized additives exhibited excellent thermal stability, with thermal decomposition temperatures exceeding 230 °C. Initial oxidation temperature tests demonstrated that the synthetic additives can improve the oxidation stability of the base oil.

Tribological test results showed that these three additive molecules not only possess outstanding extreme-pressure properties but also exhibit remarkable anti-wear and friction-reducing effects under point-to-point friction conditions. Under the ball-on-flat reciprocating sliding mode, all three additives exhibited relatively superior friction-reducing properties. With increasing temperature, the friction-reducing performance of PDM-DBDTC and BZT-DBDTC remained stable, with the wear scar diameter at 150 °C reduced by 51.59% and 54.12%, respectively, versus the neat base oil.

Analysis of the friction surface reveals that the strategic incorporation of polar functional groups enhances the adhesion of additive molecules on the metal surface and accelerates the efficiency of chemical film formation during friction. The active sulfur elements within the additive molecules undergo tribochemical reactions with the metal surface, forming a chemical reaction film composed of sulfides, inorganic sulfates, oxides, and related compounds. This film effectively prevents direct contact between the friction pairs.

Supplementary Materials: The following supporting information can be downloaded at https://www.mdpi.com/article/10.3390/lubricants14010035/s1. Figure S1. ^{1}H NMR spectra of (a1) Py-2- DBDTC, (b1) PDM-DBDTC, and (c1) BZT-DBDTC; ^{13}C NMR spectra of (a2) Py-2- DBDTC, (b2) PDM-DBDTC, and (c2) BZT-DBDTC. Figure S2. MS spectra of (a) Py-2- DBDTC, (b) PDM-DBDTC, and (c) BZT-DBDTC. Result of copper corrosion: Figure S3. (a)–(e): From left to right are commercial additive DBDTC, PDM-DBDTC, Py-2-DBDTC, and BZT-DBDTC. Figure S4. Different mass fractions of (a) the average wear spot diameter of Py-2- DBDTC, PDM-DBDTC, BZT-DBDTC and DBDTC; (b) the average coefficient of friction of Py-2-DBDTC, PDM-DBDTC, BZT-DBDTC and DBDTC; (c): the PB of PDM-DBDTC, Py-2-DBDTC, BZT-DBDTC and DBDTC. Figure S5. XPS survey spectrum. Table S1. Summary of copper strip corrosion ratings.

Author Contributions: Conceptualization, M.W. and T.L.; methodology, W.H.; validation, M.W. and T.L.; formal analysis, M.W. and T.L.; investigation, M.W. and T.L.; resources, M.W. and T.L.; data curation, M.W. and T.L.; writing—original draft preparation, M.W. and T.L.; writing—review and editing, W.H.; supervision, J.W., W.H., and J.L.; project administration, Z.L., W.H., and J.L. All authors have read and agreed to the published version of the manuscript.

Funding: The authors would like to thank "The Key Project of the Henan Province Science and Technology Research and Development Joint Funds (235200810015)" and "International Partnership Program of Chinese Academy of Sciences (307GJHZ2022034GC)" for their financial support for this work.

Data Availability Statement: The data presented in this study are available in the article.

Conflicts of Interest: The authors declare no conflicts of interest.

References

1. Sirorattanakul, K.; Larochelle, S.; Rubino, V.; Lapusta, N.; Rosakis, A.J. Sliding and Healing of Frictional Interfaces That Appear Stationary. *Nature* **2025**, *639*, 947–953. [CrossRef]
2. Gao, Q.; Liu, S.; Huang, Y.; Hou, K.; Li, Z.; Wang, J.; Yang, S. Macroscale and Durable Near-Zero Wear Performance on Steel Surfaces Achieved by Natural Ternary Deep Eutectic Solvents. *J. Mater. Chem. A* **2024**, *12*, 21799–21812. [CrossRef]
3. Luo, J. Investigation on the Origin of Friction and Superlubricity. *Chin. Sci. Bull.* **2020**, *65*, 2966–2978. [CrossRef]
4. Liu, H.; Yang, B.; Wang, C.; Han, Y.; Liu, D. The Mechanisms and Applications of Friction Energy Dissipation. *Friction* **2023**, *11*, 839–864. [CrossRef]

5. Jin, B.; Chen, G.; He, Y.; Zhang, C.; Luo, J. Lubrication Properties of Graphene under Harsh Working Conditions. *Mater. Today Adv.* **2023**, *18*, 100369. [CrossRef]
6. Tomanik, E.; Christinelli, W.; Souza, R.M.; Oliveira, V.L.; Ferreira, F.; Zhmud, B. Review of Graphene-Based Materials for Tribological Engineering Applications. *Eng* **2023**, *4*, 2764–2811. [CrossRef]
7. Mariño, F.; del Río, J.M.L.; López, E.R.; Fernández, J. Chemically Modified Nanomaterials as Lubricant Additive: Time Stability, Friction, and Wear. *J. Mol. Liq.* **2023**, *382*, 121913. [CrossRef]
8. Kumar, S.; Saha, A. Effects of Particle Size on Structural, Physical, Mechanical and Tribology Behaviour of Agricultural Waste (Corncob Micro/Nano-Filler) Based Epoxy Biocomposites. *J. Mater. Cycles Waste Manag.* **2022**, *24*, 2527–2544. [CrossRef]
9. Saini, V.; Seth, S.; Ramakumar, S.S.V.; Bijwe, J. Carbon Nanoparticles of Varying Shapes as Additives in Mineral Oil Assessment of Comparative Performance Potential. *ACS Appl. Mater. Interfaces* **2021**, *13*, 38844–38856. [CrossRef]
10. Qiu, F.; Feng, W.; Song, H.; Yang, Z.; Zhang, F.; Hu, X. On the Structure–Activity Relationship of Glyceryl Oleate Friction Modifiers and Its Synergistic Mechanism on Phosphate Ester Antiwear Additives. *Tribol. Lett.* **2023**, *71*, 90. [CrossRef]
11. Uzoma, P.C.; Hu, H.; Khadem, M.; Penkov, O.V. Tribology of 2D Nanomaterials: A Review. *Coatings* **2020**, *10*, 897. [CrossRef]
12. Kumara, C.; Meyer, H.M., III; Qu, J. Material-Dependent Antagonistic Effects between Soot and ZDDP. *Adv. Mater. Interfaces* **2020**, *7*, 1901956. [CrossRef]
13. Povar, I.; Spinu, O. Forecasting Chemical Synergism and Antagonism by Thermodynamic Analysis of Complex Equilibria in Metal Solvent Extraction. *Chem. Eng. J. Adv.* **2025**, *23*, 100825. [CrossRef]
14. Biresaw, G.; Compton, D.; Evans, K.; Bantchev, G.B. Lipoate Ester Multifunctional Lubricant Additives. *Ind. Eng. Chem. Res.* **2016**, *55*, 373–383. [CrossRef]
15. Upadhyay, M.; Karmakar, G.; Kapur, G.S.; Ghosh, P. Multifunctional Greener Additives for Lubricating Oil. *Polym. Eng. Sci.* **2018**, *58*, 810–815. [CrossRef]
16. Su, H.; Zhao, Q.; Chen, Y.; Zhao, Q.; Jiang, C.; Lou, W. Synthesis and Investigation of Phosphorus-Free Ionic Liquids as Multifunctional Lubricating Additives. *RSC Adv.* **2022**, *12*, 25134–25142. [CrossRef]
17. Chen, Y.; Renner, P.; Liang, H. A Review of Current Understanding in Tribochemical Reactions Involving Lubricant Additives. *Friction* **2023**, *11*, 489–512. [CrossRef]
18. Mittal, P.; Rai, H.; Kumari, S.; Khatri, O.P.; Gosvami, N.N. Efficient Friction and Wear Reduction of Al-Si Alloy via Tribofilms Generated from Synergistic Interaction of ZDDP and Chemically Functionalized h-BN Additives. *Appl. Surf. Sci.* **2022**, *595*, 153520. [CrossRef]
19. Spikes, H. Mechanisms of ZDDP—An Update. *Tribol. Lett.* **2025**, *73*, 38. [CrossRef]
20. Zhao, Y.; Geng, Z.; Li, D.; Wang, L.; Lu, Z.; Zhang, G. An Investigation on the Tribological Properties of Graphene and ZDDP as Additives in PAO4 Oil. *Diam. Relat. Mater.* **2021**, *120*, 108635. [CrossRef]
21. Kim, Y.-W.; Chung, K.; Kim, N.-S.; Hwang, D.-H.; Cho, W.-O. Synergistic Lubricating Effect of Several Ashless Dithiocarbamates with Mo-Donor Additives. *Tribol. Int.* **2007**, *40*, 397–404. [CrossRef]
22. Yan, J.; Zeng, X.; van der Heide, E.; Ren, T. The Tribological Performance and Tribochemical Analysis of Novel Borate Esters as Lubricant Additives in Rapeseed Oil. *Tribol. Int.* **2014**, *71*, 149–157. [CrossRef]
23. Qiao, R.; Li, J.; Wu, H.; Ren, T.; Zhao, Y.; Ma, C. The Tribological Chemistry of the Triazine Derivative Additives in Rape Seed Oil and Synthetic Diester. *Appl. Surf. Sci.* **2011**, *257*, 3843–3849. [CrossRef]
24. Xue, W.; Ma, W.; Xu, X.; Li, T.; Zhou, X.; Wang, P. Synthesis and Properties of Thiadiazole Lubricant Additives. *Ind. Lubr. Tribol.* **2017**, *69*, 891–896. [CrossRef]
25. Zhang, J.; Hu, W.; Li, J. Enhanced Tribological Performance of Melamine Long-Chain Alcohol Esters in High-Temperature Boundary Lubrication. *Lubricants* **2025**, *13*, 114. [CrossRef]
26. Zeng, X.; Li, J.; Wu, X.; Ren, T.; Liu, W. The Tribological Behaviors of Hydroxyl-Containing Dithiocarbamate-Triazine Derivatives as Additives in Rapeseed Oil. *Tribol. Int.* **2007**, *40*, 560–566. [CrossRef]
27. Xiong, L.; He, Z.; Han, S.; Tang, J.; Wu, Y.; Zeng, X. Tribological Properties Study of N-Containing Heterocyclic Imidazoline Derivatives as Lubricant Additives in Water-Glycol. *Tribol. Int.* **2016**, *104*, 98–108. [CrossRef]
28. *ASTM E2009-08 (2014)*; Standard Test Methods for Oxidation Onset Temperature of Hydrocarbons by Differential Scanning Calorimetry. ASTM International: West Conshohocken, PA, USA, 2014.
29. *GB/T 5096-2017*; Test Method for Corrosiveness to Copper from Petroleum Products by Copper Strip Test. Standards Press of China: Beijing, China, 2017.
30. *GB/T 3142—2019*; Determination of Load-Carrying Capacity of Lubricants—Four-Ball Method. Standards Press of China: Beijing, China, 2019.
31. *ASTM D2783-21*; Standard Test Method for Measurement of Extreme-Pressure Properties of Lubricating Fluids (Four-Ball Method). ASTM International: West Conshohocken, PA, USA, 2021.
32. *NB/SH/T 0189—2017*; Standard Test Method for Wear Preventive Characteristics of Lubricating Fluid—Four-Ball Method. China Petrochemical Press: Beijing, China, 2017.

33. Lewis, R.; Olofsson, U. Mapping Rail Wear Regimes and Transitions. *Wear* **2004**, *257*, 721–729. [CrossRef]
34. *ASTM G133*; Standard Test Method for Linearly Reciprocating Ball-on-Flat Sliding Wear. ASTM International: West Conshohocken, PA, USA, 2022.
35. Nath, A.R.; Yehye, W.A.; Zulkifli, N.; Johan, M.R. Ester of Thiolated Butylated Hydroxytoluene: Potential Antioxidant for Synthetic Lubricant Oil. *Thermochim. Acta* **2018**, *670*, 7–12. [CrossRef]
36. Chen, J.; Xu, X.; Zeng, X.; Feng, M.; Qu, R.; Wang, Z.; Nesnas, N.; Sharma, V.K. Ferrate(VI) Oxidation of Polychlorinated Diphenyl Sulfides: Kinetics, Degradation, and Oxidized Products. *Water Res.* **2018**, *143*, 1–9. [CrossRef]
37. Li, H.; Zhang, Y.; Li, C.; Zhou, Z.; Nie, X.; Chen, Y.; Cao, H.; Liu, B.; Zhang, N.; Said, Z.; et al. Extreme Pressure and Antiwear Additives for Lubricant: Academic Insights and Perspectives. *Int. J. Adv. Manuf. Technol.* **2022**, *120*, 1–27. [CrossRef]
38. Ma, R.; Zhao, Q.; Zhang, E.; Zheng, D.; Li, W.; Wang, X. Synthesis and Evaluation of Oil-Soluble Ionic Liquids as Multifunctional Lubricant Additives. *Tribol. Int.* **2020**, *151*, 106446. [CrossRef]
39. Gao, X.; Liu, D.; Song, Z.; Dai, K. Isosteric Design of Friction-Reduction and Anti-Wear Lubricant Additives with Less Sulfur Content. *Friction* **2018**, *6*, 164–182. [CrossRef]
40. Johnson, B.; Wu, H.; Desanker, M.; Pickens, D.; Chung, Y.-W.; Wang, Q.J. Direct Formation of Lubricious and Wear-Protective Carbon Films from Phosphorus- and Sulfur-Free Oil-Soluble Additives. *Tribol. Lett.* **2017**, *66*, 2. [CrossRef]
41. Alves, S.M.; Schroeter, R.B.; dos Santos Bossardi, J.C.; de Andrade, C.L.F. Influence of EP Additive on Tool Wear in Drilling of Compacted Graphite Iron Influence of EP Additive on Tool Wear in Drilling of Compacted Graphite Iron. *J. Braz. Soc. Mech. Sci. Eng.* **2011**, *33*, 197–202. [CrossRef]
42. Wang, H.; Wang, Y.; Wen, P.; Ma, L.; Fan, M.; Dong, R.; Zhang, C. Low-Viscosity Oligoether Esters (OEEs) as High-Efficiency Lubricating Oils: Insight on Their Structure–Lubricity Relationship. *Friction* **2024**, *12*, 1133–1153. [CrossRef]
43. Chadha, N.; Sharma, R.; Saini, P. A New Insight into the Structural Modulation of Graphene Oxide upon Chemical Reduction Probed by Raman Spectroscopy and X-Ray Diffraction. *Carbon Lett.* **2021**, *31*, 1125–1131. [CrossRef]
44. Erdemir, A.; Ramirez, G.; Eryilmaz, O.L.; Narayanan, B.; Liao, Y.; Kamath, G.; Sankaranarayanan, S.K.R.S. Carbon-Based Tribofilms from Lubricating Oils. *Nature* **2016**, *536*, 67–71. [CrossRef]
45. Qiao, D.; Wang, H.; Feng, D. Benzimidazolyl Phosphates as Anti-wear Additives in Poly(Ethylene Glycol) for Steel/Steel Contacts. *Lubr. Sci.* **2013**, *26*, 1–11. [CrossRef]
46. Huang, W.; Hou, B.; Zhang, P.; Dong, J. Tribological Performance and Action Mechanism of S-[2-(Acetamido) Thiazol-1-Yl] Dialkyl Dithiocarbamate as Additive in Rapeseed Oil. *Wear* **2004**, *256*, 1106–1113. [CrossRef]

Disclaimer/Publisher's Note: The statements, opinions and data contained in all publications are solely those of the individual author(s) and contributor(s) and not of MDPI and/or the editor(s). MDPI and/or the editor(s) disclaim responsibility for any injury to people or property resulting from any ideas, methods, instructions or products referred to in the content.